Unconventional superconductivity in weakly correlated, non-centrosymmetric Mo_3Al_2C

E. Bauer,[1] G. Rogl,[2] Xing-Qiu Chen,[3] R.T. Khan,[1] H. Michor,[1] G. Hilscher,[1]
E. Royanian,[1] K. Kumagai,[4] D.Z. Li,[3] Y.Y. Li,[3] R. Podloucky,[2] and P. Rogl[2]

[1]*Institute of Solid State Physics, Vienna University of Technology, A-1040 Wien, Austria*
[2]*Institute of Physical Chemistry, University of Vienna, A-1090 Wien, Austria*
[3]*Shenyang National Laboratory for Materials Science,*
Institute of Metal Research, Chinese Academy of Sciences, Shenyang, China
[4]*Division of Physics, Graduate School of Science,*
Hokkaido University, Sapporo, 060-0810, Japan
(Dated: February 15, 2022)

Electrical resistivity, specific heat and NMR measurements classify non-centrosymmetric Mo_3Al_2C (β-Mn type, space group $P4_132$) as a strong-coupled superconductor with $T_c = 9$ K deviating notably from BCS-like behaviour. The absence of a Hebbel-Slichter peak, a power law behaviour of the spin-lattice relaxation rate (from ^{27}Al NMR), a T^3 temperature dependence of the specific heat and a pressure enhanced T_c suggest unconventional superconductivity with a nodal structure of the superconducting gap. Relativistic DFT calculations reveal a splitting of degenerate electronic bands due to the asymmetric spin-orbit coupling, favouring a mix of spin-singlet and spin triplet components in the superconducting condensate, in absence of strong correlations among electrons.

PACS numbers: 74.25.Bt, 74.70.Ad, 72.15.Eb

Carbides based on Mo comprise a large body of refractory compounds, where carbon atoms (in trigonal prismatic or octahedral Mo_6C subunits) occupy a fraction of the interstitial sites either in an ordered or in a random manner. Among Mo-based carbides for which superconductivity (SC) was reported (αMoC at $T_c = 9.95$ K, ηMoC at 7.57 K, Mo_2BC at 6.33 K and Mo_3Al_2C at 9.05 K) the crystal structure of Mo_3Al_2C is outstanding, since the respective β-Mn type does not possess a center of inversion [1]. The missing inversion symmetry might initiate a mixture of spin-singlet and spin-triplet pairs in the SC condensate [2] as was recently proposed to explain SC in $CePt_3Si$ [3], UIr [4], $CeRhSi_3$ [5], and $CeIrSi_3$ [6]. Non-centrosymmetry (NCS) of the crystal structure introduces an electrical field gradient and, thereby, creates a Rashba-type antisymmetric spin-orbit coupling [2].

The Ce and U-based SCs indicated above are characterised by heavy fermion behaviour at low temperatures provoked by Kondo interaction. NCS in such systems can lead to new anomalous spin fluctuations, stabilizing triplet pairing, in addition to the singlet part [7]. On the other hand, a variety of SCs has been identified, which lacks strong electron correlations as well as a centre of inversion. For a recent listing of these systems see Ref. [8]. Except Li_2Pt_3B [9], all yet studied NCS SCs without strong correlations among electrons are typical s-wave fully gapped BCS SC either weakly or strongly coupled.

In order to shed light onto the primary mechanism activating unconventional SC, we are searching for systems where SC occurs in absence of inversion symmetry, and also in absence of strong electron correlations. Revisiting Mo_3Al_2C (β-Mn structure), we aim to extend research done in the 1960's [10], providing insight into microscopic features and the electronic structure.

For the preparation of Mo_3Al_2C an elemental powder mixture (purity > 99.9 mass%, about 5 g) was cold compacted, reacted in a high vacuum furnace for 24 hrs at 1500°C with one intermediate grinding and compacting step. Afterwards the material was ball milled and hot pressed at 1250°C at 56 MPa. Refinement of the crystal structures was performed with the program Fullprof [11]. Measurements of physical properties were carried out with standard techniques [12, 13]. The density functional theory (DFT) calculations were performed with the *Vienna ab initio Simulation Package* (VASP) [14]. For details see our recent paper on NCS $BaPtSi_3$ [8].

X-ray Rietveld refinement confirmed a cubic, non-centrosymmetric structure (space group $P4_132$), isotypic to the β-Mn type; see Fig. 1).

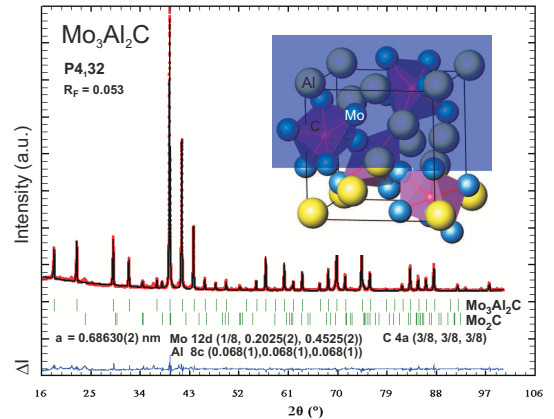Measurements of the temperature dependent electrical resistivity ρ of Mo_3Al_2C clearly evidences metallic be-

FIG. 1: Rietveld refinement (Guinier-Huber image plate system, $CuK_{\alpha 1}$) and crystallographic data of Mo_3Al_2C. The inset shows a 3-dimensional view of the crystal structure. Traces of Mo_2C are indicated by vertical bars.

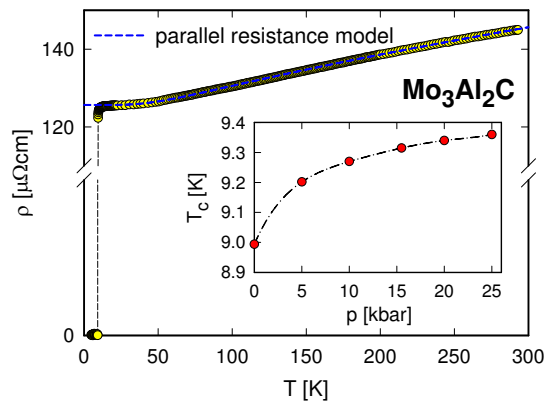FIG. 2: (Color online) Temperature dependent electrical resistivity ρ of Mo_3Al_2C. The dashed line is a least squares fit according to the parallel resistance model. The inset shows the pressure dependence of T_c.

FIG. 3: (Color online) (a) Temperature dependent specific heat C_p of Mo_3Al_2C plotted as C_p/T vs. T^2. The dashed line is a guide for the eye and indicates an idealised superconducting phase transition together with a T^3 dependence of $C_p(T)$ for $T < T_c$. The solid line represents $C_p(T)$ of a spin-singlet fully gapped BCS superconductor according to Mühlschlegel [19]. (b) Temperature dependent $1/T_1$ ^{27}Al relaxation rate deduced at $\mu_0 H = 1.24$ and 6.95 T. The solid lines are guides for the eye. The dashed line represents an exponential temperature dependence.

haviour and indicate a SC phase transition at $T_c = 9$ K (see Fig. 2), in agreement with the data reported by Johnston et al. [15]. SC with almost 100 % volume fraction is revealed from magnetic susceptibility measurements as well. Since the absolute resistivity values are large, the parallel resistance model (compare e.g., Ref. [16]) can be used to describe $\rho(T)$, where the ideal resistivity follows from the Bloch-Grüneisen model. A fit employing this model is shown in Fig. 2 as a solid line, revealing a Debye temperature $\theta_D = 286$ K and a saturation value $\rho_{sat} = 350$ $\mu\Omega$cm. An estimation of the electron-phonon interaction strength $\lambda_{e,ph}$ is possible in terms of the McMillan formula [17]. Applying this model, and taking the repulsive screened Coulomb part $\mu^* \approx 0.13$, yields $\lambda_{e,ph} \approx 0.8$; this characterizes Mo_3Al_2C as a SC well beyond the weak coupling limit.

The pressure dependence of T_c of Mo_3Al_2C is displayed in the inset of Fig. 2. Obviously, $T_c(p)$ increases, but tends to saturate for high pressures. An increase of T_c is rarely found in a simple materials; rather, such a behaviour frequently occurs in unconventional SCs like in high temperature SCs, in various pyrochlores, in some Fe-pnictides or heavy fermion materials. Bogolyobov et al. [18] demonstrated that there are two principal parameters determining T_c: θ_D and the electronic density of states at the Fermi energy, $N(E_F)$. Since the application of pressure hardly modifies $\rho(T, p)$ in the normal state region (not shown here), $\theta_D(p)$ remains unchanged. Thus, a slight increase of $N(E_F)$ is concluded, enhancing T_c on pressurizing Mo_3Al_2C.

Fig. 3 shows the temperature dependent specific heat C_p of Mo_3Al_2C taken at 0 T and plotted as C_P/T vs. T^2. Bulk SC is evidenced from a distinct anomaly at 9 K, rendering the onset of the SC phase transition. A closer inspection of the data gives evidence of various non-BCS like features: i) The jump of the specific heat at T_c, $\Delta C_p/(\gamma_n T_c) \approx 2.28$, is well above the value expected for an s-wave BCS SC with $\Delta C_p/(\gamma T_c) \approx 1.43$. This
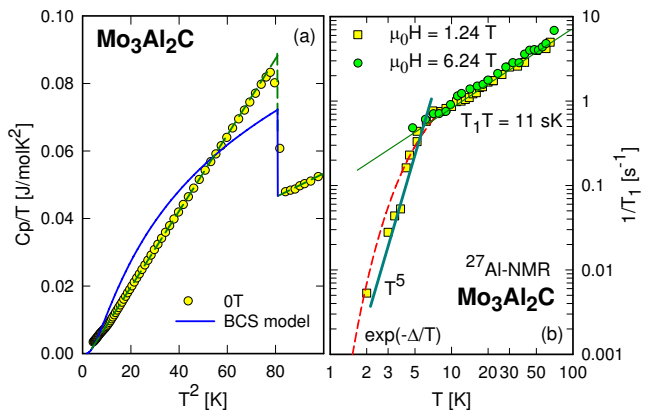
clearly evidences strong-coupling SC. ii) The temperature dependent heat capacity below T_c significantly deviates from the universal BCS dependence as indicated by the solid line. Rather, a power law with $C_p(T < T_c) \propto T^3$ is obvious from the experimental data (compare Fig. 3), which is sketched by the dashed line as well. Such a temperature dependence excludes a fully gapped SC state; instead, a nodal structure is likely, where the SC gap vanishes along points.

The $1/T_1$ ^{27}Al relaxation rate, taken at $\mu_0 H = 1.24$ T and partially at 6.95 T is plotted in Fig. 3(b) on a double logarithmic scale. A Hebbel-Slichter peak right at T_c is absent. This is compatible with a partial disappearance of the SC gap at the Fermi energy, in line with non-s-wave

TABLE I: Normal state and SC properties of Mo_3Al_2C.

| crystal structure	cubic, β-Mn type
space group	$P4_132$
lattice parameter	$a = 0.68630$ nm
Sommerfeld value	$\gamma_n = 17.8$ mJ/molK^2
Debye temperature	$\theta_D = 315$ K
transport mean free path	$\lambda_{tr} = 3.06$ nm
transition temperature	$T_c = 9.0$ K
electron-phonon enhancement factor	$1 + \lambda_{e,ph} = 1.8$
upper critical field	$\mu_0 H_{c2}(0) \approx 15.7$ T
slope of upper critical field	$\mu_0 H'_{c2} = -3$ T/K
thermodynamic critical field	$\mu_0 H_c(0) = 0.146$ T
correlation length	$\xi \simeq 4.6$ nm
Ginzburg Landau parameter	$\kappa_{GL} \simeq 76$
London penetration depth	$\lambda \simeq 380$ nm
nodal structure	point-nodes
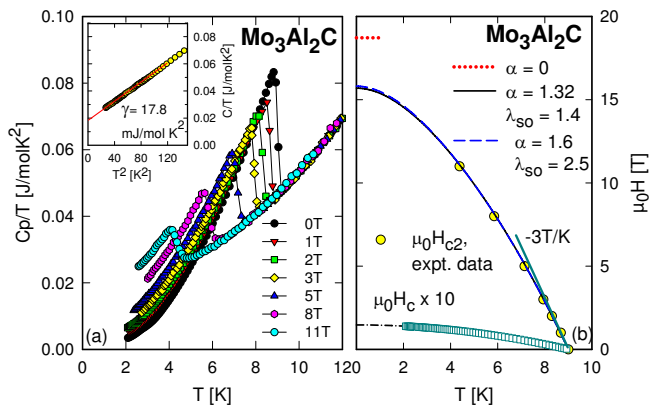
FIG. 4: (Color online) (a) Temperature and field dependent specific heat C_p of Mo$_3$Al$_2$C. (b) Temperature dependent upper critical field $\mu_0 H_{c2}$ and thermodynamic critical field $\mu_0 H_c$ as obtained from specific heat measurements. The solid and the long-dashed lines are fits according to the WHH model for different values of the Maki parameter. The horizontal bar indicates the upper critical field $\mu_0 H^*(0)$ in absence of Pauli-limiting. The dashed-dotted line is an extrapolation of the thermodynamic critical field towards zero.

SC. Below T_c, a non-exponential but rather a T^n temperature dependence hints towards a nodal structure, closing partially the SC gap at the Fermi surface. We note that a $1/T_1 \propto T$ component, expected as a signature of a finite impurity density of states, is clearly absent in our low temperature data. Volovik and Gork'ov [20] have shown that a proportionality of the density of states according to $N(E) \propto E^m$ results in a NMR relaxation rate $1/T_1 \propto T^{2m+1}$. Thus, an anisotropic gap with nodal structures yields, in general, a T^n power law of $1/T_1$ with $n = 3$ for line nodes and $n = 5$ for point nodes. Intersecting nodes, however, might modify such simple temperature dependencies [21]. Furthermore, Hayashi et al. [22] demonstrated that NCS SCs with mixed spin singlet and triplet states infer a rather unconventional $1/T_1$ relaxation rate.

Summarized in Fig. 4(a) is the field and temperature dependent heat capacity of Mo$_3$Al$_2$C, highlighting the suppression of SC upon the application of a magnetic field. The fact that even fields of 11 T do not suppress superconductivity evidences a large upper critical field $\mu_0 H_{c2}$ as well as a large initial slope $\mu_0 H'_{c2}$. The extension of the normal state behaviour towards lower temperatures with rising magnetic fields allows to obtain in a standard manner the Sommerfeld value $\gamma = 17.8$ mJ/molK^2 and $\theta_D \approx 315$ K (compare Fig. 4(a), inset). The accurate determination of γ and of $T_c(\mu_0 H)$ was accomplished by idealizing the heat capacity anomaly under the constraint of entropy balance between the superconducting and the normal state. $T_c(\mu_0 H)$ obtained from Fig. 4(a) is plotted in Fig. 4(b).

The temperature dependency of $\mu_0 H_{c2}$ is described following the model of Werthammer et al. [23], incorporating orbital pair-breaking, the effect of Pauli spin

paramagnetism and spin-orbit scattering. Two parameters, the Maki parameter α (Pauli paramagnetic limitation) [24] and spin-orbit scattering λ_{so} specify this model. While an increase of α decrements the upper critical field, an increase of λ_{so} compensates the former, restoring for $\lambda_{so} \to \infty$ a maximum field constrained from orbital pair breaking only. In a first approximation, the Maki parameter α can be derived from γ and ρ_0 [23], resulting in $\alpha = 1.32$. Alternatively, α can be estimated from $\mu_0 H'_{c2}$ [24], revealing $\alpha^* = 1.6$. The sizable Maki parameter of both approximations is an indication that Pauli limiting is non-negligible in Mo$_3$Al$_2$C.

Using $\alpha = 1.32$ ($\alpha^* = 1.6$) and $\mu_0 H'_{c2} = -3$ T/K yields $\mu_0 H_{c2}(T)$ as displayed as solid and dashed lines in Fig. 4(b) for $\lambda_{so} = 1.4$ and $\lambda_{so} = 2.5$, respectively, with $\mu_0 H_{c2}(0) \approx 15.7$ T. The Pauli limiting field follows from $\mu_0 H_p(0) = \sqrt{2}\mu_0 H^*(0)/\alpha$, where $\mu_0 H^*(0) = 18.72$ T, is the WHH result for $\alpha = 0$, i.e., the orbital limit. Thus, $\mu_0 H_p(0) = 20$ T for the former and 16.5 T for the latter value of α. These values are in line with $\mu_0 H_p(1.2$ K$) = 15.6$ T reported by Fink et al. [25]. In the case of strong coupling superconductivity, these values are further en-
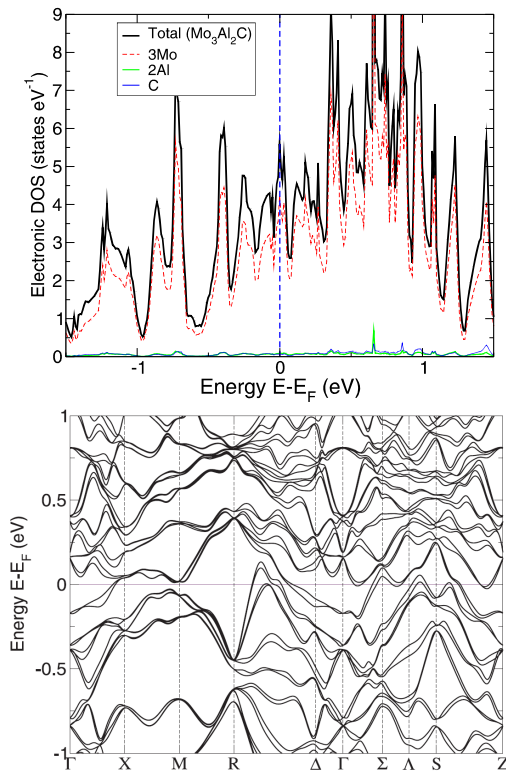

FIG. 5: (Color online) (Upper panel) Section of relativistic total and atom-projected densities of states (DOS) in states eV^{-1} for Mo$_3$Al$_2$C summed over all three Mo atoms for the energy range ± 1.5 around the Fermi energy E_F. (Lower panel): Relativistic electronic band structure along high symmetry directions for Mo$_3$Al$_2$C in the energy range $\pm 1.$ eV around the Fermi energy E_F.

hanced according to $H_p^{str}(0) = H_p(0)(1 + \lambda_{e,ph})^\epsilon$ with $\epsilon = 0.5$ or 1.0 [26, 27]. Hence, Pauli limiting is not the principal mechanism restricting the upper critical field in Mo_3Al_2C, but is present in a relevant size.

The thermodynamic critical field $\mu_0 H_c(T)$ derived from heat capacity data (compare e.g. Ref. [8]) is shown in Fig. 4(b) by open squares; an extrapolation to $T \to 0$ (dashed-dotted line) yields $\mu_0 H_c(0) \approx 0.146\,\mathrm{T}$.

SC and normal state parameters of Mo_3Al_2C can be assessed from γ, $\mu_0 H'_{c2}$, $\mu_0 H_{c2}(0)$ and ρ_0 [26, 28]. From the Ginzburg Landau theory with the thermodynamic critical field as primary input, the coherence length, the Ginzburg Landau parameter and the London penetration depth are calculated. Parameters are summarized in Table I. Based on the estimate $l_{tr}/\xi \approx 0.66$ we classify Mo_3Al_2C as a superconductor in the dirty limit; $\kappa_{GL} \approx 76$ refers to a type II superconductor.

A section of the calculated electronic density of states (DOS) of Mo_3Al_2C is shown in Fig. 5 for a relativistic calculation including spin orbit coupling (upper panel). The DOS around the Fermi energy stems primarily from from Mo-$4d$ states, whilst the contribution of Al and C is almost negligible. The low partial Al DOS calculated at E_F corresponds well to the NMR Korringa constant, $T_1 T = 11$ sK ($1/T_1 T \propto N(E_F)^2$). A comparison with Al metal ($T_1 T = 1.8$ sK) reveals a local Al DOS in Mo_3Al_2C of about 3 % with respect to the total DFT DOS.

The Fermi energy E_F of Mo_3Al_2C is located in a local maximum of the DOS; its large value favours SC. Employing the Sommerfeld expansion, $N(E_F) = 5.48$ states/eV corresponds to $\gamma_b = 12.9$ mJ/molK^2, in fair agreement with $\gamma = \gamma_b(1 + \lambda_{e,ph}) = 17.8$ mJ/molK^2.

The lower panel of Fig. 5 displays the DFT electronic band structures along high symmetry directions for Mo_3Al_2C. With respect to a non-relativistic calculation (not shown here), the degenerate bands become split due to the lack of inversion symmetry in Mo_3Al_2C.

Specifically, for all bands crossing the Fermi energy the degeneracy is lifted, separating spin-up and spin-down electrons. This provides conditions for the occurrence of spin-singlet and spin-triplet Cooper pairs, leading to two gap functions, where each gap is defined on one of the two bands formed by degeneracy lifting. Superposition of these gaps is presumed to constitute a nodal structure of the resulting SC gap as corroborated from the present experimental data.

In conclusion, electrical resistivity, specific heat and NMR measurements classify non-centrosymmetric Mo_3Al_2C as a strong-coupled SC with $T_c = 9$ K. The temperature dependent specific heat and the $1/T_1$ ^{27}Al NMR relaxation rate deviate from BCS predictions, thus referring to a nodal structure of the superconducting gap even though SC of Mo_3Al_2C occurs in the dirtly limit. This manifests a robustness of the unconventional order parameter of the NCS superconductor. Moreover, unconventional pairing is in line with the splitting of electronic bands due to the asymmetric spin-orbit coupling as revealed from relativistic DFT calculations. These split bands might be the cause of a mixing of spin-singlet and spin-triplet Cooper pairs, which otherwise are distinguished by parity [2], making a nodal structure likely [22, 29]. Whilst this proposition has been corroborated for SCs with strong correlations among electrons, specific heat data unambiguously disprove a strongly correlated electronic state in Mo_3Al_2C. In spite of a lack of correlations, unconventional SC seems to arise from a substantial band splitting and the fact that inversion symmetry is missing in *all* crystallographic directions. In these respects, Mo_3Al_2C is the only example besides isomorphous Li_2Pt_3B [9].

[1] L.E. Toth and J. Zbasnik, Acta Met., **16**, 1177 (1968).
[2] L.P. Gor'kov and E.I. Rashba, Phys. Rev. Lett. **87**, 037004 (2001).
[3] E. Bauer *et al.*, Rev. Lett., **92**, 027003 (2004) .
[4] T. Akazawa *et al.*, J. Phys.: Cond. Mat. **16**, L29 (2004).
[5] N. Kimura *et al.*, Phys. Rev. Lett. **95**, 247004 (2005).
[6] I. Sugitani *et al.*, J. Phys. Soc. Japan **75**, 043703 (2006).
[7] T. Takimoto and P. Thalmeier, J. Phys. Soc. Japan, **78**, 103703 (2009).
[8] E. Bauer *et al.*, Phys. Rev. B, **80**, 064504 (2009).
[9] H. Q. Yuan *et al.*, Phys. Rev. Lett. **97**,017006 (2006).
[10] L. E. Toth, in *Transition Metal Carbides and Nitrides*, Refractory Materials, Vol.7, A Series of Monographs, Ed. J.L. Margrave, Acad Press Inc., NY & London, 1971
[11] J. Rodriguez-Carvajal, Physica B **192**, 55 (1993).
[12] E. Bauer *et al.*, Phys. Rev. B **66**, 214421 (2002).
[13] E. Bauer *et al.*, Phys. Rev. B **76**, 014528 (2007).
[14] G. Kresse and J. Furthmüller, Phys. Rev. B **54**, 11169 (1996); G. Kresse and D. Joubert, Phys. Rev. B **59**, 1758 (1996).
[15] J. Johnston *et al.*, Solid State Commun., **2**, 123 (1964).
[16] O. Gunnarsson *et al.*, Rev. Mod. Phys. **75**, 1085 (2003).
[17] W. L. McMillan, Phys. Rev. **167**, 331 (1968).
[18] N.N. Bogoliubov et al., Fortschr. Physik **6**, (1958) 605.
[19] B. Mühlschlegel, Z. f. Physik **155**, 313 (1959).
[20] G.E. Volovik and L.P. Gork'ov, Sov. Phys.-JETP **61**, 843 (1985).
[21] Y. Hasegawa, J. Phys. Soc. Japan, **65**, 3131 (1996).
[22] N. Hayashi *et al.*, Phys. Rev. B **73**, 092508 (2006).
[23] N.R. Werthamer *et al.*, Phys. Rev. **147**, 295 (1966).
[24] K. Maki, Phys. Rev. **148**, 362 (1966).
[25] H.J. Fink *et al.*, Phys. Rev. **138**, A1170 (1965).
[26] T.P. Orlando *et al.*, Phys. Rev. B **19**, 4545 (1979).
[27] M. Schossmann and J.P. Carbotte, Phys. Rev. B 39, 4210 (1989)
[28] See, for example M. Tinkham, *Introduction to Superconductivity*, McGraw-Hill, New York, 1975.
[29] P. A. Frigeri *et al.*, Phys. Rev. Lett. **92**, 097001 (2004).